AL-SIC INTERFACE STRUCTURE STUDIED BY HREM

VANDENBURG, M; DEHOSSON, JTM; Burg, M. van den

Published in:
Acta Metallurgica et Materialia

DOI:
10.1016/0956-7151(92)90287-O

Publication date:
1992

Acta metall. mater. Vol. 40, Suppl., pp. S281–S287, 1992
Printed in Great Britain.

0956-7151/92 $5.00 + 0.00

Al–SiC INTERFACE STRUCTURE STUDIED BY HREM

M. VAN DEN BURG and J. Th. M. DE HOSSON

Department of Applied Physics, Materials Science Centre, University of Groningen, Nijenborgh 18, 9747 AG Groningen, The Netherlands

Abstract—A comparison is made between the two well-known aluminium alloys 2014 and 6061, cold pressed from powder and subsequently extruded, with and without a reinforcement of 30 wt% α-SiC particulates. The former one has a strength of 550 MPa and a strain at fracture of 1% while the latter one has a more moderate strength of 415 MPa but a fracture strain of 4%. A high resolution electron microscopy study of the Al–SiC interface indicates that proper wetting is achieved in both alloys. A preferred orientation relationship is observed in the 6061–SiC combination: $(0001)_{SiC}//\{111\}_{Al}$; $\langle 2\bar{1}\bar{1}0\rangle_{SiC}//\langle 110\rangle_{Al}$. When the $(0001)_{SiC}$ is not parallel to the interface, a stepped interface is observed with the 6061 alloy, with one part of the step parallel to the SiC basal plane and one type of the Al octahedral planes and the other part parallel to another type of Al octahedral planes. In the 2014 alloy the steps seem to be less pronounced probably due the processing route.

Résumé—On effectue une comparaison entre deux alliages d'aluminium bien connus 2014 et 6061 comprimés à froid à partir de poudres, puis extrudés avec ou sans renfort de 30% en poids de particules de SiC-α. Le premier a une résistance mécanique de 550 MPa et une déformation à la rupture de 1% tandis que le second a une résistance mécanique plus modérée de 415 MPA, mais une déformation à la rupture de 4%. Une étude par microscopie électronique en haute résolution de l'interface Al/SiC indique qu'un mouillage correct est réalisé dans les deux alliages. Une relation d'orientation préférentielle est observée dans la combinaison 6061/SiC: $(0001)_{SiC}//\{111\}_{Al}$; $\langle 2\bar{1}\bar{1}0\rangle_{SiC}//\langle 110\rangle_{Al}$. Lorsque le $(0001)_{SiC}$ n'est pas parallèle à l'interface, une interface avec des marches est observée pour l'alliage 6061, avec une partie des marches parallèle au plan basal de SiC et à un type de plans octaédriques d'Al, et l'autre partie parallèle à un autre type de plans octaédriques d'Al. Dans l'alliage 2014, les marches semblent moins prononcées, probablement par suite de la méthode d'élaboration.

Zusammenfassung—Zwei gut bekannte Aluminiumlegierungen, 2014 und 6061, die aus Pulver kaltverpreßt und danach extrudiert worden sind, mit oder ohne Verstärkung durch 30 Gew. α-SiC-Teilchen, werden miteinander verglichen. Di Legierung 2014 weist eine Festigkeit von 550 MPa und eine Bruchdehnung von 1% auf, wohingegen die Legierung 6061 eine eher mäßige Festigkeit von 415 MPa, aber eine Bruchdehnung von 4% aufweist. Die Analyse der Al/SiC-Grenzfläche wird im hochauflösenden Elektronenmikroskop analysiert; es ergibt sich eine gute Benetzung in beiden Legierungen. Bei der Kombination 6061/SiC findet sich eine bevorzugte Orientierungsbeziehung: $(0001)_{SiC}//\{111\}_{Al}$; $\langle 2\bar{1}\bar{1}0\rangle_{SiC}//\langle 110\rangle_{Al}$. Liegt $(0001)_{SiC}$ nicht parallel zur Grenzfläche, dann wird in der Legierung 6061 eine gestufte Grenzfläche beobachtet, wobei ein Teil der Stufe parallel zur Basisebene des SiC und einm Typ der Al-Oktaederebenen, der andere Teil parallel zu einem anderen Typ der Al-Oktaederebenen verläuft. In der Legierung 2014 scheinen die Stufen weniger ausgeprägt zu sein, wahrscheinlich wegen der gewählten Herstellbedingungen.

1. INTRODUCTION

In research on metal–matrix composites one often concentrates on the interface as being the most crucial parameter through which the improvement in strength should be achieved. In this report we compare two composites in which the reinforcement is kept the same, namely 30 wt% α-SiC, but the metal–matrix is either 2014 or 6061. As a result we should be able to compare the interface strength with the matrix strength.

However, one should bear in mind that in general metal–matrix composites are characterized by heterogeneity, anisotropy and interfaces [1]. Consequentially, in a description of their mechanical properties one should be aware of the considerable complexities associated with the microstructural features. Nevertheless, one may say that the adhesion between matrix and inclusions in a particle composite material is one of the principal factors which determine the mechanical behaviour of the composite material. Further insight into the mechanisms contributing to metal–non metal adhesion requires investigations by which information on an atomic level is obtained.

The present study reports, beside some mechanical properties, a high resolution electron microscopy study (HREM) of interfaces in two commercial aluminium-based metal–matrix composites with α-SiC particulates. Aluminium alloys reinforced with ceramic particles belong to a class of materials with

Table 1. Composition of the aluminium alloys 6061 and 2014 (wt%)

	Cu	Fe	Mg	Mn	Si	Zn	Cr	Al
Al 6061	0.29	0.02	1.09	0.005	0.60	0.002	0.18	Bal.
Al 2014	4.78	0.04	0.8	0.79	0.66	0.018	—	Bal.

the potentiality for high strength to weight ratio, together with a good creep resistance and toughness at elevated temperatures. The paper treats the interfacial structure in two different aluminium alloys, 2014 and 6061, the compositions of which are listed in Table 1.

2. MECHANICAL PROPERTIES

The 2014 alloy derives its strength from the formation of Guinier Preston zones in which copper is precipitating between $\{100\}_{Al}$ planes. Subsequently, these zones grow out to coherent Θ'' platelets in a very dense maze type pattern marked in the electron microscope by internal misfit stresses. A rather large number of bigger, incoherent precipitates are also observed. They turn out to be either Al_2Cu (Θ) or MnSi precipitates, but occasionally also Fe and Cr containing precipitates were observed as was checked by X-ray elemental analysis. They are probably not a dominant factor in the strength build-up but they may be instrumental in the low strain at fracture.

The 6061 alloy derives its strength from Mg_2Si precipitates, which form as needles in $\langle 100 \rangle_{Al}$ directions in approximately the same density as the previously mentioned Θ'' precipitates but they are not coherent and do not constitute such strong barriers for dislocation movement [2]. In comparison with 2014 almost no big precipitates were found inside the matrix grains, only on grainboundaries. Table 2 lists the mechanical properties of the two alloys both with and without 30 wt% SiC particulates as reinforcement.

From this table it is obvious that the UTS for the unreinforced 2014 alloy is already considerably higher than the one for the unreinforced 6061 alloy. The reinforcement represents a medium improvement in this respect. As an additional feature Table 2 also lists the effect of a change in temperature for the solid solution treatment. The change in UTS levels off with increasing solid solution temperature for 6061; not so, however, for 2014 for which alloy the strength continues to increase even when the temperature is already outside the temperature range of the α phase situated between 492 and 507°C for this composition [3]. Calorimetric scans (DSC) do show a small endothermic peak at 518°C probably as indication that the solidus temperature was surpassed and a big peak and 645°C as indication of the liquidus temperature. These peaks were observed both in the reinforced and in the unreinforced specimens, while no such peaks could be detected in the scans for the 6061 or 6061–SiC samples. The literature values for solidus and liquidus temperatures are 507 and 638°C for 2014 and 582 and 652°C for 6061, respectively [3]. The discrepancy between experiment and literature may be due to differences in scanning rates.

The reason for the increase in mechanical strength with solution temperature may find an explanation in the fact that the matrix becomes partly liquid, the wetting angle drops and a reaction occurs with surrounding particles, until then protected by a thin oxide layer. The reaction layer, often of spinel structure, may constitute a stronger bond [4]. Dahl and Johnsen [5] found an optimum heat treatment of 5 h at 540°C in a similar study on a Al–4 wt% Cu alloy.

With respect to the SiC particulates, also here only the liquid may react and form Al_4C_3. The excess Si may harden the matrix by forming extra Mg_2Si precipitates but at the same time the reinforcement is disintegrating. Al_4C_3 is metastable and reacts further to Al_2O_3.

It is against this background that we decided to investigate the interface between the aluminium matrix and the ceramic reinforcement with high resolution electron microscopy.

3. SPECIMEN PREPARATION

The composite material in the extruded endform was obtained from the Materials Development Group at Billiton/Shell Research BV, Arnhem-NL. 2014 and 6061 were fabricated via powder metallurgical processing, i.e. via degassing, cold isostatic pressing and extrusion of powder. The solid solution treatment and ageing were done in air as well as in

Table 2. Mechanical properties of the aluminium alloys 2014 and 6061 with and without a reinforcement of 30 wt% SiC

	Solid solution temperature (°C)	Ultimate tensile strength (MPa)	Strain at fracture (%)
Al 2014	480	441	9.1
	500	508	9.4
	520	552	10.1
Al 2014 + 30 wt% SiC	480	490	1.3
	500	530	1.4
	520	574	0.8
Al 6061	520	224	14.1
	540	373	12.3
	560	370	13.6
Al 6061 + 30 wt% SiC	520	393	4.4
	540	411	3.4
	560	419	4.0

Fig. 1. High resolution electron micrograph of an Al–SiC interface in 2014 with both the $(0001)_{SiC}$ and the $\{111\}_{Al}$ lattice fringes resolved.

an inert atmosphere. In particular the solution treatment of 3 h at 520°C of the 2014 alloy turned out to be quite sensitive for the atmosphere during the heat treatment. In a protected atmosphere only medium degradation of the sample material took place while in air the extruded bar showed a kind of additional degassing sometimes even forming large bubbles underneath the surface and disintegration at some locations inside. Secondary electron images of a sample heat treated at 550°C revealed conglomerates of small particles at SiC sites. On these sites X-ray elemental analysis indicated a higher than normal amount of oxygen. To circumvent these problems it may be necessary to increase the degassing temperature of the powder and reduce the time for the solid solution treatment. After water quenching and ageing for 15 h at 180°C, the samples were ready to be prepared for the transmission electron microscope.

Crucial to the experiment is the preparation of the sample for the electron microscope. The specimens, 3 mm in diameter and 0.5 mm thick, were cut by spark erosion. Subsequently, they were thinned by grinding and dimpling on both sides to a remaining thickness of 20 μm and were further thinned by micro ion milling with a 4 kV argon ion beam under an angle of 8° and given a final electrochemical treatment. It turned out to be necessary during the ion milling to check the samples from time to time by putting them into the microscope in order to see whether both the SiC reinforcement and the neighbouring Al matrix were sufficiently transparent. According to the literature, higher angles resulted in serious preferential thinning due to much higher thinning rate of aluminium than SiC [6]. Several electron microscopes, as there are the Akashi 002B and the Philips CM30 ST were used, operating at 200 keV and 300 keV, respectively.

4. RESULTS

In Fig. 1 an Al–SiC interface in the 2014 sample is imaged in which the lattice fringes of the octahedral plane of the aluminium matrix as well as the basal plane of the SiC reinforcement are resolved. A typical diffraction pattern of such an interface is depicted in Fig. 2. It represents a superposition of the $(2\bar{1}\bar{1}0)_{SiC}$ and the $(22\bar{1})_{Al}$ foil plane patterns so that the $[0001]_{SiC}$ direction makes an angle of 20° with the $[1\bar{1}0]_{Al}$ direction. As is clear from the micrograph no reaction layer, amorphous or crystalline, can be detected, so that it can be concluded that good wetting is achieved.

In Fig. 3 6061–SiC interface is depicted in which both the $\{200\}_{Al}$ and the $(0001)_{SiC}$ fringes are imaged.

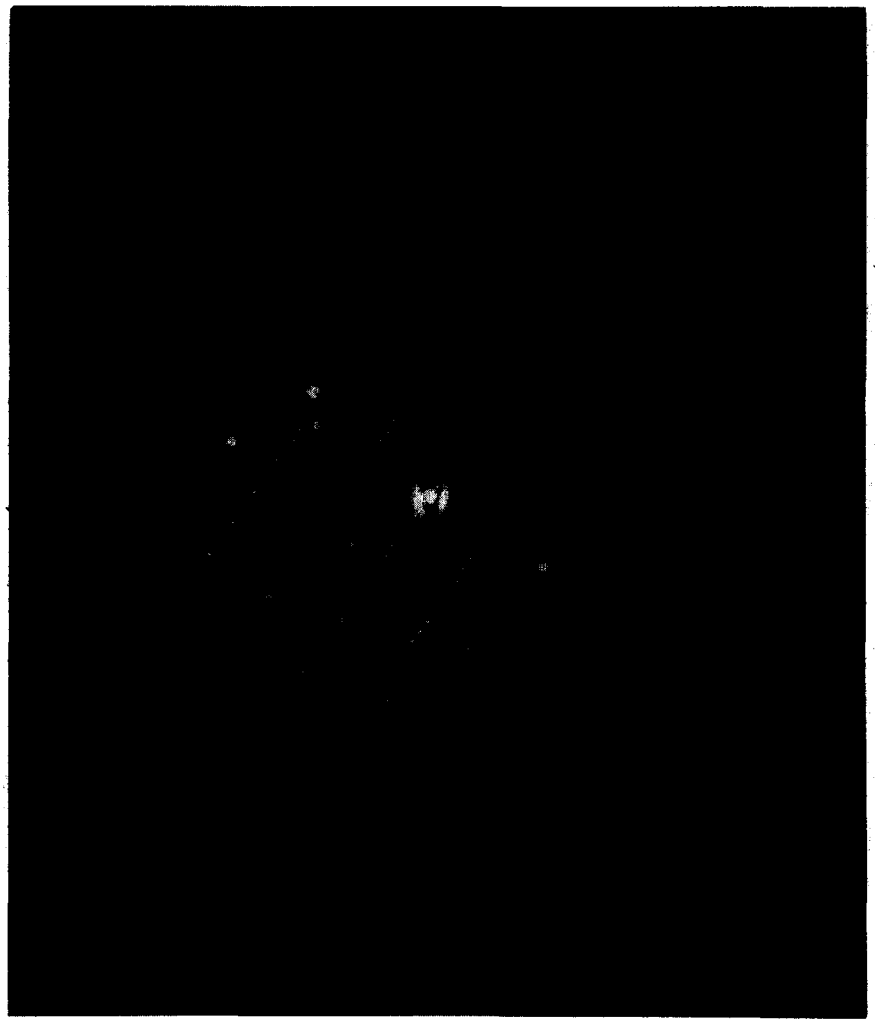

Fig. 2. Diffraction pattern of an Al–SiC interface in 2014 showing a superposition of the $(2\bar{1}\bar{1}0)_{SiC}$ and $(22\bar{1})_{Al}$ foil plane patterns.

The SiC structure is two dimensionally resolved and the typical chevron like structure of the hexagonal SiC-6h structure (Fig. 4), imaged in a $\langle 2\bar{1}\bar{1}0\rangle$pole, can be seen. The $(001)_{SiC}$ basal plane is parallel to the interface between the Al and the SiC. At some places the $\{200\}_{Al}$ lattice fringes are resolved but the different thinning rates of the aluminium and the silicon carbide causes the aluminium to be very thin at places where the SiC lattice can be imaged. Either the oxidation of the Al causes the loss of fringe resolution or the damage caused by ion milling. It turns out that the $\{111\}_{Al}$ plane fringes are also parallel to that surface.

The $\{200\}_{Al}$ fringes, imaged in a$\langle 110\rangle$ pole, make an angle of 54° with the interface which means there is a $\{111\}_{Al}$ octahedral plane parallel to the interface with a$\langle 110\rangle_{Al}$ parallel to a$\langle 2\bar{1}\bar{1}0\rangle_{SiC}$. The lattice parameter for the $\langle 110\rangle_{Al}$ is 0.286 nm and for the $\langle 2\bar{1}\bar{1}0\rangle_{SiC}$ is 0.307 nm giving rise to a 7% misfit based on geometrical arguments. Other resolved patches of aluminium show $\{200\}_{Al}$ lattice fringes which are incompatible with each other indicating that the aluminium matrix near the SiC particle may be heavily deformed by ion milling.

In 6061–SiC it is observed that the $(0001)_{SiC}$ is not always parallel to the interface (Fig. 5). Instead a stepped surface can be found. One face of this step is parallel to the $(0001)_{SiC}$. The other face of the step seems to follow the $\{10\bar{1}1\}_{SiC}$ prismatic plane making an angle of 71° with the basal plane. The steps are dictated by the orientation of the $(0001)_{SiC}$ and the closer the interface is parallel to the $(0001)_{SiC}$ the wider the steps become.

5. DISCUSSION

It is illustrative to compare the 2014–SiC interface with the 6061–SiC interface. The 2014 material has entered the melting range during the solution treatment as is indicated by a small peak in a SDC measurement at 518°. As a consequence the interface in 2014–SiC does not exhibit clear steps like those that appeared in the 6061–SiC material, although one

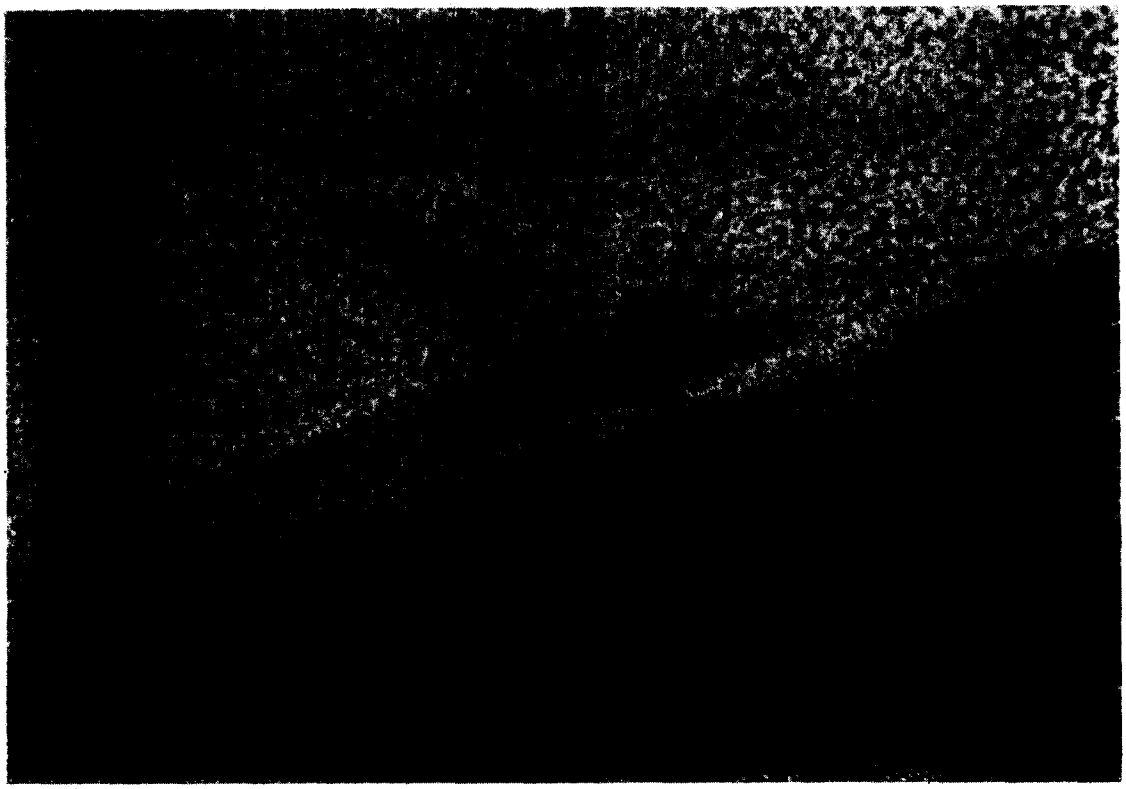

Fig. 3. High resolution electron micrograph of an Al–SiC interface in 6061 with both the $(0001)_{SiC}$ and the $\{200\}_{Al}$ lattice fringes resolved ($\langle 110\rangle$ pole).

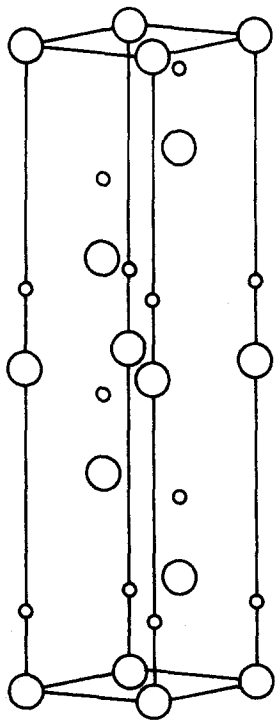

Fig. 4. The SiC unit cell with the characteristic CABC'B'A'C stacking spanning a distance of 1.5 nm. The large spheres represent the Si, the small ones the C atoms.

should keep in mind that facets may not be visible in Fig. 1 due to overlapping matrix in this case.

The main high resolution electron microscopy result is the observation that the wettability of the two alloys seem to be equally good. Figure 3 has indicated that an interface is flat when both the basal plane of SiC and the octahedral plane of the aluminium matrix are parallel to it. The observed orientation relationship deduced is: $(0001)_{Al}//\{111\}_{Al}$; $\langle 2\bar{1}\bar{1}0\rangle_{SiC}//\langle 110\rangle_{Al}$. To establish this relationship both the crystallographic structure and the α-SiC spacings were used as calibration, together with the observed angles of 54° of the $\{200\}_{Al}$ with the interface.

Similar results were reported by Withers *et al.* [7]. However, these authors preferred to use dark field electron microscopy because high resolution micrographs may suggest a diffuse interface layer while in reality one is looking at a properly wetted surface with facets in the direction of observation.

Because the lattice parameter of the $\langle 110\rangle_{Al}$ is 0.286 nm and of the $\langle 2\bar{1}\bar{1}0\rangle_{SiC}$ is 0.307 nm there is a 7% misfit based on geometrical arguments. In order to preserve the orientation relationship over longer distances there should be a dislocation every 4.2 nm. This dislocation network is not observed in the micrographs (Fig. 3) but this is probably due to the badly resolved fringes on the interface.

Fig. 5. High resolution electron micrograph showing of an Al–SiC interface in 6061 not parallel to the $(0001)_{SiC}$ basal plane.

The expected dislocations in the network that accommodates the lattice mismatch between these two close-packed planes are edge dislocations, i.e. they lie along $\langle 112 \rangle$ directions of their interface plane and their Burgers vectors are $1/2\ \langle 110 \rangle$. Examination along the $\langle 110 \rangle$ direction does not allow the observation of the complete network since they are not parallel to the incident beam. The network of the misfit dislocations will be hexagonal [11][12] and will have the symmetry of the interface with a point group 3. In the observation with the incident beam direction along the $\langle 110 \rangle$ however, two sets of misfit dislocations are inclined to it by 30° and one would have a line vector perpendicular to the incident beam direction. Consequentially, the strain fields of the inclined dislocations will necessarily affect the lattice fringe contrast.

The other possibility of course would be a less efficient dislocation network consisting of 60° dislocations. In this case both the dislocations and Burgers vectors would run into the $\langle 110 \rangle$ directions and the network would become visible in the HREM images taking the incident beam along a $\langle 110 \rangle$ direction parallel to the interface. This, however, is not observed although this possibility cannot be excluded because of the insufficient contrast at the interface.

When the $\{200\}_{Al}$ planes make an angle of 67° (Fig. 6) with the interface an extended type of interfacial dislocation can be found. From the observations it is not clear whether the interface in fact consists of $\{111\}_{Al}//(0001)_{SiC}$ with $\langle 110 \rangle_{Al}//\langle 2\bar{1}\bar{1}0 \rangle_{SiC}$. As far as the misfit is concerned, in that case one would expect extended dislocation contrast along 1.2 and 2.5 nm apart because of the inclination of the dislocations by 30° as is suggested by the observations. On the other hand $\{200\}_{Al}$ planes do not make angles of 67° with $\{111\}$ planes. So, one might

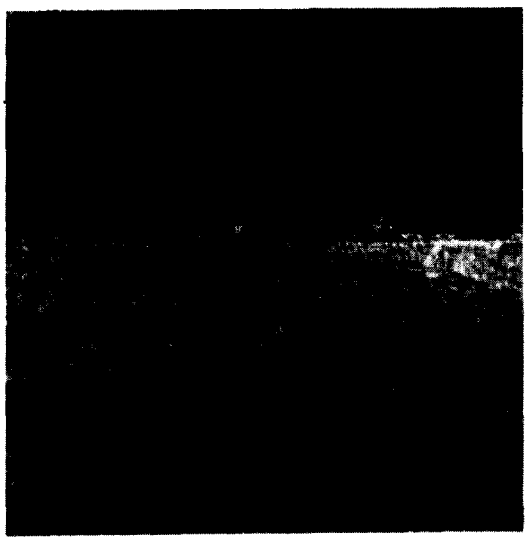

Fig. 6. High resolution electron micrograph of an Al–SiC interface in 6061 with the $(0001)_{SiC}$ and the $\{200\}_{Al}$ fringes resolved.

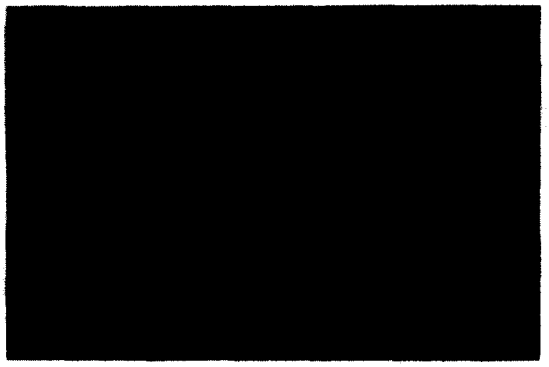

Fig. 7. On the interface a patch of SiO_2 is visible.

think that during the processing step of 6061–SiC diffusion of Al onto SiC has led to an epitaxial layer whereas the adjacent Al matrix is heavily defective.

The SiC particles are manufactured by crushing larger particles to an average particle size of 9 μm. The silicon carbide seems to have a tendency to fracture along $(0001)_{SiC}$ planes. Whenever the geometry does not allow such an orientation steps are formed after processing with one face of the step parallel to the basal plane and one face along a less well defined orientation. The steps are most distinct at places where a reaction took place.

Such an area is depicted in Fig. 7. It contains lattice fringes with a spacing of 0.33 nm parallel to the $\{10\bar{1}1\}_{SiC}$ plane and fringes with a spacing of 0.25 nm parallel to the $(0001)_{SiC}$ planes. This corresponds to the hexagonal alpha-quartz SiO_2 phase imaged in the $\langle 10\bar{1}1\rangle$ direction. Formation of a SiO_2 layer on the SiC interface has been reported [10] for preparation by the liquid route but in our case no continuous layer could be detected suggesting that preparation by the powder metallurgical route gives less reaction on the interface. No orientation relation could be observed between the Al matrix and the SiO_2 particle.

This is in contrast to the observations of 2014–SiC. When the aluminium matrix passes the solidus temperature during the preparation, as in the case of our 2014, no orientation relation could be observed between the SiC particle and the Al matrix. The reaction that may occur during the treatment is [9]: $4Al + 3SiC \rightarrow Al_4C_3 + 3Si$. Al_4C_3 is metastable and may react further to Al_2O_3.

The growth of Al_4C_3 as a continuous layer will be dominated by a solid state diffusion through it. One would expect a more rapid growth normal to the prism planes of SiC because of a more open interfacial structure of the side faces leading to less distinct edges along the prism planes. The latter is indeed observed (Fig. 1). In addition, when the rate limiting step is the dissolution from the close-packed basal planes, a SiC surface with an average orientation that is initially non-basal will become rough on a macroscale and facetted along basal and prism planes on an atomic scale.

6. CONCLUSION

In conclusion we may state that HREM observations of the Al–SiC interfaces in 6061–SiC and 2014–SiC indicate that proper wetting between the Al and the SiC is achieved. In the 6061–SiC composite a preferred orientation relationship is deduced: $(0001)_{SiC}//\{111\}_{Al}$; $\langle 2\bar{1}\bar{1}0\rangle_{SiC}//\langle 110\rangle_{Al}$. If the $(0001)_{SiC}$ is not parallel to the interface a stepped interface is observed in the 6061 alloy. In the 2014 alloy the steps seem to be less pronounced because of reactions taken place at the interface during processing.

As indicated in Table 2 the UTS of unreinforced 2014 is much higher than the UTS of unreinforced 6061, while the strain at fracture, as measure for the ductility, is larger for the latter one. From the same table it is obvious that with reinforcement these differences are raised by the same amount. The improvement due to the SiC is modest if compared with the existing differences in the unreinforced alloys. The high resolution lattice imaging results indicate no interface regions present.

Acknowledgements—This work is part of the research program of IOP-Metalen (C89 427 RG XX), The Hague, The Netherlands and of the Foundation for Fundamental Research on Matter (FOM-Utrecht) and has been made possible by financial support from the Netherlands Organization for Research (NWO-The Hague). We like to thank Drs J. L. Hutchison, M. Otten and P. Keppler for their involvement in taking the high resolution micrographs and EDS spectra.

REFERENCES

1. *Interfaces in Metal–Matrix Composites* (edited by A. K. Dhingra and S. G. Fishman). Am. Inst. Min. Engrs, New York (1986).
2. P. Haasen, *Physic . Metallurgy*. Cambridge Univ. Press (1978).
3. F. King, *Aluminium and its Alloys*. Ellis Horwood, Chichester (1987).
4. V. Laurent, D. Chatain and N. Eustathopoulos, *Mater Sci. Engng A* **135**, 89 (1991).
5. N. Dahl and T. E. Johnsen, *Mater. Sci. Engng A* **135**, 151 (1991).
6. D. O. Karlsen *et al.*, *Mechanical and Physical Behaviour of Metallic–Ceramic Composites* (edited by S. I. Andersen).
7. P. J. Withers, W. H. Stobbs and J. Bourdillon, *J. Microsc.* **151**, 159. (1988).
8. R. C. Pond, in *Dislocations in Solids* (edited by F. R. N. Nabarro), Vol. 8, p. 1. North-Holland, Amsterdam (1969).
9. P. Piroux, F. Ernst, in *Metal-Ceramic Interfaces* (edited by I. M. Rühle, A. G. Evans, M. C. Ashby and J. P. Hirth), p. 199. Pergamon Press, Oxford (1990).
10. R. Warren and C. H. Andersson, *Composites* **15**, 101 (1984).
11. T. Iseki, T. Kameda and T. Maruyama, *J. Mater. Sci.* **19**, 1692. (1984).
12. C. Handwerker, M. D. Vandin, U. R. Kattner and D.-J. Lee, in *Metal-Ceramic Interfaces* (edited by M. Rühle, A. G. Evans, M. F. Ashby and J. P. Hirth), p. 129. Pergamon Press, Oxford (1990).